Digital Image Analysis to Assess Microbubble Behavior in Porous Media

By S. E. Burns,[1] Associate Member, ASCE, and M. Zhang,[2] Student Member, ASCE

Abstract: Air sparging is a commonly implemented technology for the remediation of volatile organic compounds from contaminated soil and ground water. In the sparging process, air is pressurized into the soil/groundwater matrix through injection wells. The air then travels to the ground surface through buoyancy, acting as a collector for volatile chemicals. To date, the design and implementation of air sparging has been largely empirical, based on the results of pilot studies. This paper uses digital image analysis to examine the transport and coalescence behavior of microbubbles in porous media, one of the most important control parameters for contaminant removal in air sparging. This laboratory study compared the diameter of bubbles produced in aqueous systems with the diameters produced in uniform spherical particulate media (diameters of 14.5 mm and 27.0 mm) and in elliptically shaped particulate media (equivalent spherical diameters of 14.5 mm). Results showed that the presence of a particulate media increased the average diameter and also increased the range of diameters of bubbles produced during sparging. As the diameter of the particulate media increased, the size of the bubbles decreased, indicating less coalescence in media with larger pore space. In addition, the effect of trace concentrations of surface-active agents (surfactants) on the diameter and coalescence behavior of bubbles was examined. In both aqueous and aqueous/particulate matrices, the presence of surfactants significantly decreased the average diameter of the bubbles produced. Additionally, the degree of coalescence decreased in the surfactant systems, producing a very narrow range of bubble diameters in both aqueous and aqueous/particulate media.

INTRODUCTION

Air sparging is rapidly becoming one of the most commonly implemented remediation methods for the removal of volatile organic compounds (VOCs) from contaminated soil and ground water. The sparging process is essentially a stripping technique that mobilizes contaminants to the vapor phase through mass transfer into air bubbles. The process also stimulates biological degradation of contaminants through the introduction of oxygen into the ground water, a process known as biosparging. In the sparging process, air is pressurized into ground water through an injection well with porous openings. The gas travels through the soil/ground water in the form of either discrete bubbles or channels of air. Contaminants transfer into the vapor phase due to the concentration gradient and migrate to the surface through buoyancy. The VOC-laden vapor is then collected at the soil surface using soil vapor extraction (SVE), and treated for the removal of organics. While air sparging is being implemented at many field sites it is still a relatively new method, and implementation of the process to date has largely been empirical, based on the results of pilot studies (Marley et al. 1992). The initial implementation of air sparging systems has proven that the technique is a viable one; however, a more fundamental understanding of the parameters that control remedial performance is required in order to provide more efficient and cost-effective designs. One of the most important aspects of the sparging process is that of the characteristics of the stripping gas introduced into the contaminated media. This paper uses digital image analysis to quantify the effect of a porous medium on the growth and transport of mechanically produced bubbles; it also analyzes the effect of surfactants on the behavior of microbubbles.

Fundamental to the success of air sparging is the delivery of gas bubbles for volatilization, with the objective being the mass transfer of VOCs to the gaseous phase. Ideally, implementation of the process is achieved through a uniform distribution of gas bubbles throughout the subsurface; however, experimental evidence suggests that significant channeling of gas flow occurs when a gas is sparged into a porous media, especially when low permeability lenses are present (Baker et al. 1995; Leeson et al. 1995). Current methods of bubble generation in sparging processes involve the mechanical pressurization of air, or another gas, into the contaminated ground water through a porous well screen. However, it is well documented in the literature that the size of the bubbles produced during the mechanical sparging of air is large when compared with other methods of bubble generation (Burns et al. 1997). Large bubbles are a disadvantage in stripping operations because the low surface area-to-volume ratios limit mass transfer into and out of the vapor phase. In air sparging applications, the smaller microbubbles are advantageous in the remedial process because small diameter bubbles have high surface area-to-volume ratios that facilitate mass transfer, are less buoyant, and have a longer residence in the system—having dimensions approximating those of the porous media, which facilitates transport through the pore network.

Alternately, small amounts of a surface-active agent (surfactant) can be used to produce smaller diameter gas bubbles in a porous medium. Surfactants are soaps, detergents, or long-chain alcohols that tend to accumulate at the interface between different phases. Because they can increase the apparent water solubility of nonaqueous phase liquids (NAPLs) (Kile and Chiou 1989; Haulbrook et al. 1993), surfactants are being studied for use in the remediation of contaminated ground water (Smith et al. 1997). This study examines the effect of trace concentrations of surfactant on the characteristics of bubbles produced in porous media. A more fundamental understanding of the removal mechanisms active in the sparging process requires knowledge of the behavior of gaseous bubbles in a porous medium. A variety of studies, both qualitative and quantitative, have been performed to assess bubble flow behavior and bubble terminal velocity.

Wehrle (1990) performed qualitative studies on the movement of air through gravels and coarse-grained sands. The results showed that low permeability soils can develop pores that are filled with air essentially continuously, and that stratified

[1]Asst. Prof., Dept. of Civ. Engrg., Thornton Hall, Univ. of Virginia, Charlottesville, VA 22903-2442. E-mail:sburns@virginia.edu

[2]Grad. Res. Asst., Dept. of Civ. Engrg., Thornton Hall, Univ. of Virginia, Charlottesville, VA.

Note. Discussion open until June 1, 1999. To extend the closing date one month, a written request must be filed with the ASCE Manager of Journals. The manuscript for this paper was submitted for review and possible publication on October 13, 1998. This paper is part of the ***Journal of Computing in Civil Engineering***, Vol. 13, No. 1, January, 1999.

simulated porous medium. Spherical silica beads, ranging in diameter from 4.0 mm to 0.2 mm, were used as the model porous medium in a thin, two-dimensional Plexiglas test chamber. Air was injected at the bottom of the test chamber and the flow pattern of the gas was monitored using a video recorder. All experimental simulations were illuminated from the back of the chamber. Three simulations were performed with uniform packings of beads with diameters of 4.0 mm, 2.0 mm, and 0.75 mm; two simulations were performed with a mixture of bead sizes; and one simulation was performed with layered bead sizes in order to simulate low permeability zones. Ji et al. (1993) found that for uniform grain sizes with bubble diameters of approximately one to three bead diameters, air flow occurred as discrete bubbles; however, for smaller bead diameters, the flow transitioned from flow of bubbles to channelized flow through the porous medium. Additionally, the mixtures of bead sizes and layers of small diameter beads led to nonuniform flow behavior and stagnant zones that were not exposed to airflow.

Roosevelt and Corapcioglu (1998) used image analysis to measure the terminal velocity of air bubbles injected into a glass column randomly packed with 4.0 mm diameter glass beads. A single air bubble was injected into the saturated porous medium and the bubble movement up the length of the column was recorded using a camcorder. All experiments were performed using a backlit system, and the time of translation of the center of the bubble was monitored using a timer with an accuracy of 0.1 s. Image processing was used to background subtract the glass beads from successive video images. This method left an image of the moving bubble and allowed monitoring of the translation of the bubble center as a function of time. The rate of vertical rise of a bubble in a porous medium was found to be linearly dependent on time. The writers found that horizontal migration did occur but had a negligible effect on the vertical rise velocity. Additional results indicated that the rise time through a large-grained porous medium was approximately 20–25% slower than rise time through an unbounded aqueous medium, and bubble rise velocity through a capillary tube decreased significantly as the bubble diameter approached that of the tube. This is significant because bubble flow through porous media has frequently been modeled as flow through a bundle of capillary tubes (Rimmer et al. 1996).

Burns et al. (1997, 1998) used image analysis to measure the size of bubbles produced in aqueous media using mechanical and electrochemical generation techniques. The bubble images were videotaped using long-distance microscopy in combination with a video cassette recorder. Images were printed and imported into an image analysis system for determination of their equivalent circular diameter. The studies quantified differences in the bubble size, size distribution, and power consumption for bubbles generated using the different methods.

Other nonoptical imaging methods applied to monitor the transport of microbubbles through porous media include X-ray tomography (Chen et al. 1996) and electrical resistance tomography (Schima et al. 1994; Lundegard and LaBreque 1995; Bruell et al. 1997). Chen et al. (1996) used an X-ray computerized tomography (CT) medical scanner to image three-dimensional airflow patterns in uniform Ottawa sand soil deposits which allowed three-dimensional imaging of porosity and fluid saturations. The experimental results showed that in medium- to coarse-grained sands relatively few air channels are formed, and higher air injection rates enlarge and increase the number of channels, which increases air saturation. However, larger and more uniform air saturations were measured in lower permeability soils, regardless of the air-injection scenario. Electrical resistivity tomography applies electrical current across a set of electrodes and measures the voltage drop between the two points. An array of electrodes can be set up to measure the voltage drop in three dimensions, and the resistivity of the material through which the current flows can be calculated using inversion techniques. Because the resistivity of the medium is significantly affected by the concentration of air in the pore space, the method yields a global measurement of air saturation. The outer limit of influence of the sparged air is easily identifiable using resistivity techniques; consequently, the method has been applied for the delineation of radius of influence during sparging applications (Bruell et al. 1997).

Several imaging studies have used etched glass to simulate the pore distributions present in porous media. Li and Yortsos (1995a, 1995b) used etched glass to visualize bubble growth during pressure depletion from a supersaturated solution. The glass model was constructed with pore sizes in the range of 600–1200 μm and throat sizes of 100–600 μm (Satik and Yortsos 1996). The results showed that gas nucleated and clustered in a highly irregular manner in the large pore spaces, with a slow pressurization step followed by a rapid pore penetration step after the capillary barrier at the pore throat was overcome.

Because the growth and transport of gas bubbles within porous media is a complex phenomenon, study of the fundamental aspects of their behavior is critical to a more detailed understanding of the mechanisms that control the effectiveness of air sparging. Unlike previous studies, this paper presents quantitative results on bubble growth and coalescence behavior. The laboratory study addresses the effect of particle grain size on bubble growth and coalescence during transport through a porous medium; it also quantifies the effect of surfactants on the characteristics and transport behavior of bubbles produced in both aqueous solutions and saturated porous media.

MATERIALS AND METHODS

The laboratory experiments in this study were performed in a rectangular test cell constructed out of Pyrex glass (dimensions of 45 mm × 295 mm × 260 mm). The test cell had flat glass walls in order to allow visualization of the generated microbubbles without distortion of the images. The top panel of the test cell was removable in order to allow access to the cell for cleaning and for placement of the porous media (Fig. 1). A bubble diffuser (Kimax coarse frit, Fisher Scientific) was placed on the bottom of the test cell and connected to a pressure regulator (Model 10, Fairchild Industrial Products Company) using Tygon tubing. In all experiments, air pressure was regulated using a pressure control panel (Trautwein Soil Testing Equipment) with a digital readout accurate to within ±0.25%.

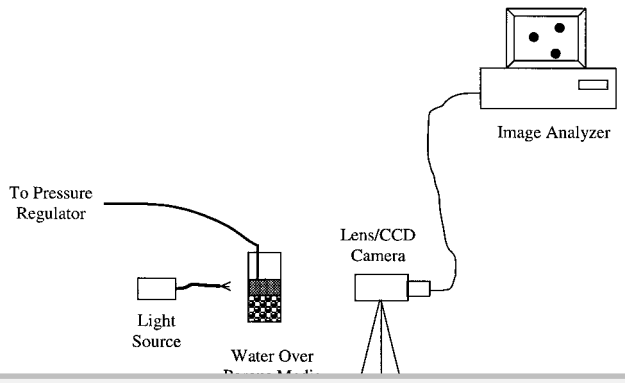

A series of experiments was performed in a deionized water medium, and another series of experiments was performed in a deionized water/silica bead media. In the aqueous experiments, the diffuser was placed in the test cell and submersed in fluid, while in the simulated soil experiments the diffuser was placed in the test cell and the silica beads carefully packed around it. In all packing procedures, the silica beads were water-wetted and placed in a small column of water in order to avoid trapped air in the void space. All specimens were packed to a porosity of approximately 40%.

Three types of silica beads were used in the study: uniform spherical beads with a diameter of 14.5 mm; uniform spherical beads with a diameter of 27.0 mm; and uniform elliptical beads with an equivalent spherical diameter of 14.5 mm (diameter to width ratio of 2:1). After placement of the silica beads, an additional 64 mm of aqueous solution was left above the porous media in order to allow visualization of the air bubbles as they emerged from the simulated soil column.

A series of experiments was performed in order to quantify the effect of surface-active agents on bubbles generated in deionized water and in deionized water and porous media. The surfactant used in the study was Triton X-100 (t-octylphenoxypolyethoxyethanol, Sigma Chemical Company), a nonionic surfactant. In all the experiments, only trace amounts of surfactant were added to the deionized water yielding a surfactant concentration of approximately 80 to 100 mg/L.

Images of bubbles produced during the experiments were captured using a long-distance microscope (model QM1, Questar) configured for magnification of approximately 40 times, in combination with a color CCD camera (model VCC-3972, Sanyo). The shutter speed on the camera was set to 1,000 frames per second. Video output from the camera was connected directly to an image acquisition board (model PCI-1408, National Instruments) installed in a Pentium II computer. A fiber-optic light was used to illuminate the experiments from behind the test cell. In this configuration, the fluid transmitted light but the bubbles did not; this provided images of dark bubbles on a light background. In order to avoid differences in bubble size due to variations in hydrostatic pressure, images of the bubbles were taken at the same height in the test cell for all experiments. In the experiments with the porous media, this corresponded to the height at which the bubbles emerged from the beads. The translation of the mobile bubbles in and out of the focal plane was a consideration in obtaining high-quality images. In all experiments the focus of the long-distance microscope was fixed, and bubble images were acquired semicontinuously, using only clear images of bubbles within the focal plane for analysis. Calibration of the system was performed by capturing an image of a wire of known diameter.

Sample gray-scale images of the bubbles produced are shown in Fig. 2(a), and the accompanying processed binary images used for measurement are shown in Figure 2(b). All image processing was performed using Scion Image for Windows (Release Beta 2, Scion Corporation). In order to reduce bias in sampling, images were snapped at random intervals, and only clearly focused images were used for processing. The gray-scale images were converted to binary images and the cross-sectional area of the bubbles was measured. All areas were converted to an equivalent circular diameter to provide uniform comparison among experiments.

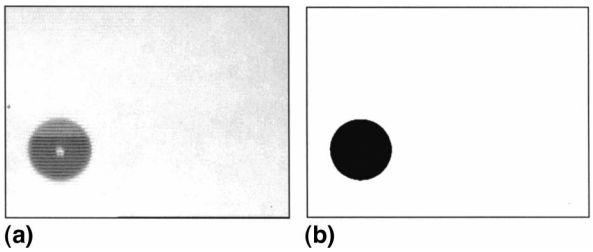

FIG. 2. Bubble Images: (a) Gray-Scale Image; (b) Binary Image

At least one hundred bubbles were analyzed in each experiment in order to obtain representative sample populations. Sample size was determined according to (Hines and Montgomery 1990):

$$n = \left(\frac{Z_{a/2}\sigma}{E}\right)^2 \quad (1)$$

where n = sample size; $Z_{a/2}$ = confidence interval; σ = standard deviation; and E = error. Table 1 gives a detailed list of the experimental conditions along with the mean bubble diameter and standard deviation for the experiments.

RESULTS

The first series of experiments measured the equivalent circular diameter of bubbles produced by mechanically pressurizing air through a bubble diffuser into deionized water. The experiments were performed in order to quantify the effect of injection pressure on the size of individual bubbles formed in the system. During this series of experiments, care was taken to ensure that no surfactant was present in the test cell. The cumulative number distribution as a function of equivalent circular diameter for the bubbles produced using injection pressures of 8.3 kPa (1.2 psi), 9.0 kPa (1.3 psi), 9.7 kPa (1.4 psi), and 11.0 kPa (1.6 psi) is shown in Fig. 3. The two distributions for the lowest pressures (8.3 and 9.0 kPa) are essentially identical with similar means (0.91 mm versus 1.05 mm), similar standard deviations (0.22 mm and 0.20 mm), and similar ranges of size (0.3 mm–2.0 mm). However, as the injection pressure is increased, three trends can be noted from the data: the average bubble diameter increases; the bubble size distribution becomes more broad with larger bubbles being pro-

TABLE 1. Summary of Experiments

Experiment number (1)	Pressure (kPa) (psi) (2)	Particle size (mm) (3)	Surfactant concentration (mg/L) (4)	Mean bubble diameter (mm) (5)	Standard deviation (mm) (6)
1	8.3 (1.2)	not applicable	not applicable	0.91	0.22
2	9.0 (1.3)	not applicable	not applicable	1.05	0.20
3	9.7 (1.4)	not applicable	not applicable	1.37	0.61
4	11.0 (1.6)	not applicable	not applicable	2.98	0.74
5	9.0 (1.3)	14.5	not applicable	2.48	1.19
6	9.0 (1.3)	27.0	not applicable	2.02	0.95
7	9.0 (1.3)	Elliptical	not applicable	2.07	0.66
8	9.7 (1.4)	not applicable	100	0.39	0.08
9	9.0 (1.3)	Elliptical	80	0.55	0.17
10	9.7 (1.4)	14.5	100	0.88	0.23
11	9.0 (1.3)	14.5	80	0.71	0.21

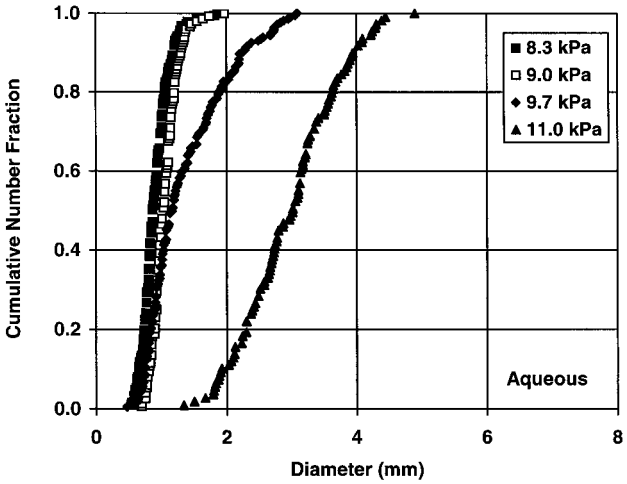

FIG. 3. Cumulative Size Distribution of Bubbles as Function of Injection Pressure

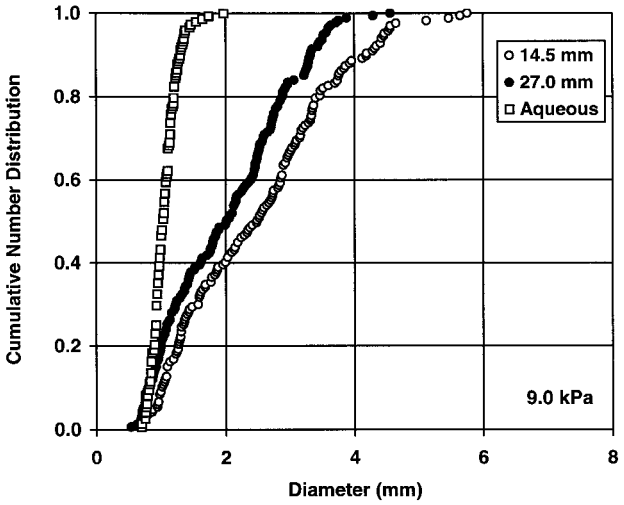

FIG. 4. Cumulative Size Distribution of Bubbles as Function of Particle Size

duced; and the entire distribution shifts toward larger diameter bubbles at the highest pressure level.

When gas is injected through an orifice into a fluid, bubble formation occurs in three distinct phases—nucleation, growth, and detachment (Lubetkin 1994). The formation of bubbles at an orifice under constant pressure conditions can be described by the following (Clift et al. 1978):

$$Q = K\left(p_{ch} - \rho gH + \rho ga - \frac{2\sigma}{a}\right)^{1/2} \quad (2)$$

where Q = flowrate; K = orifice constant; p_{ch} = chamber pressure; ρ = fluid density; g = gravitational constant; H = submergence; a = instantaneous bubble radius; and σ = surface tension. Raising the injection pressure affects the growth phase, and it increases the rate at which gas is transferred into the bubble, which increases the bubble size before it detaches (Sadhal et al. 1997).

The results of the experiments performed in spherical glass beads are shown in Fig. 4, with the results of the bubble sizes produced in an aqueous matrix shown for comparison. All experiments were performed using an injection pressure of 9.0 kPa (1.3 psi). Experiments were performed using spherical silica beads with diameters of 6.4 mm, 14.5 mm, and 27.0 mm. Only the results from the two larger diameter bead experiments are shown, because the bubbles produced in the 6.4 mm were too large to image using the test system configuration, and it wasn't possible to obtain a representative sample.

The test results in the spherical media show a significant degree of coalescence, even in beads with diameters significantly larger than most soil grains. Average bubble diameters produced were 2.48 mm (14.5 mm beads) and 2.02 mm (27.0 mm beads) which is significantly larger than the bubbles produced in aqueous media (average diameter of 1.05 mm). Previous experimental results observed discrete bubble flow in particle sizes on the order of 4.0 mm (Wehrle 1990; Ji et al. 1993); however, the results of this study show that coalescence can occur, even when the particle sizes are many times larger than the bubble diameter. It is significant to note that the bubble diameters emerging from the porous media decrease as the particle size increases. This is clear from the data for the 27.0 mm and 14.5 mm beads and is also supported by the fact that the bubbles emerging from the 6.4 mm beads were too large to capture in the imaging frame.

An experiment was performed to compare the effect of particle shape on the size of bubbles generated in the system (Fig. 5). The experiments were performed with spherically and el-

was significantly smaller in the elliptical particles than in the spherical particles (2.07 mm versus 2.48 mm), indicating a lower degree of bubble interaction and less coalescence. The difference in the distribution is most pronounced at the larger bubble sizes, with the largest bubbles having a size differential of approximately 1.5 mm.

Experiments were performed in order to evaluate the effect of low concentrations of surfactant in an aqueous system. Fig. 6 shows the results of two experiments performed at an injection pressure of 9.7 kPa, one without surfactant and one with surfactant present in the system. The presence of the surfactant makes a dramatic difference in bubble size with average diameters of 0.39 mm (standard deviation of 0.08 mm) with surfactant, and 1.37 mm (standard deviation of 0.61 mm) without surfactant. Additionally, the size distributions of the two experiments were significantly different, as reflected in the standard deviation.

Surfactants in the system cause a reduction in the interfacial tension between the fluid and the gas phases, which in turn causes a reduction in the diameter of bubbles produced under constant pressure injection scenarios (2). The accumulation of surfactants at the bubble/fluid interface also sets up a tangential force that increases the drag on the bubble (Sadhal et al. 1997), which in turn increases the bubble residence time in the system. For bubbles translating through an aqueous sys-

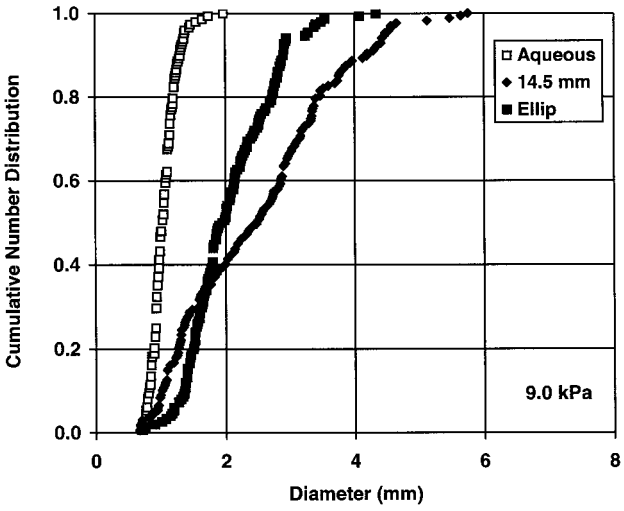

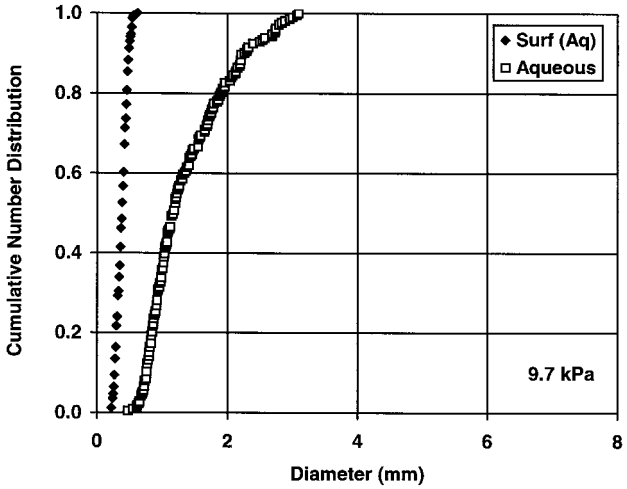

FIG. 6. Cumulative Size Distribution of Bubbles in Aqueous and Surfactant Systems

tem, the accumulation of surfactant is nonuniform, with higher concentrations at the rear of the bubble (Sadhal et al. 1997).

Figs. 7 and 8 show the results of experiments performed in aqueous/particulate media in the presence of surfactant. The data clearly show that the reduction in average bubble diameter due to the presence of surfactant occurs in particulate systems as well as in aqueous stems. In addition, the narrow size

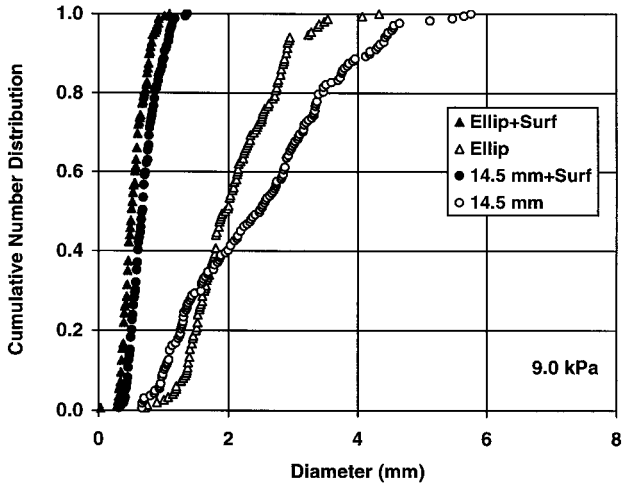

FIG. 7. Effect of Surfactant on Bubble Coalescence in Porous Media

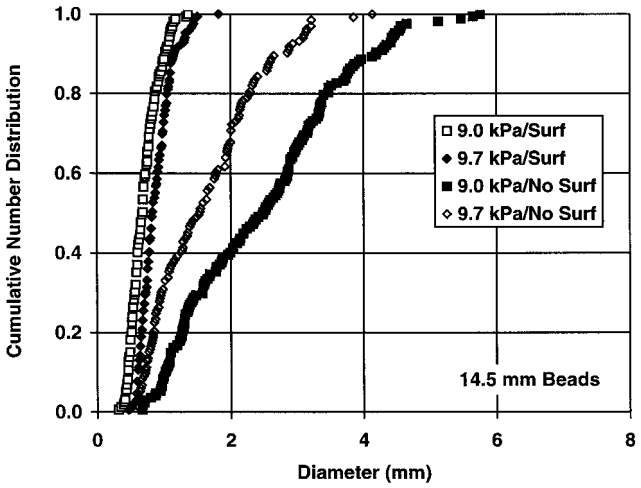

distributions show that the surfactant limits the degree of bubble coalescence in the porous media. It is interesting to note that the presence of surfactant in the system appears to dominate many of the other system variables in terms of bubble coalescence behavior. Neither the presence of the porous medium nor the increase in injection pressure had a significant impact on the size of the bubbles generated when there was surfactant present in the system.

Experimental studies detailing the effect of surfactant concentration on the contaminant removal efficiency of air sparging are ongoing (Burns and Zhang, in preparation).

CONCLUSIONS

The objective of this experimental study was to examine the characteristics of bubbles generated for application in the air sparging process. It produced quantitative measurements of bubble sizes in both aqueous and aqueous/particulate media and it quantified the effect of surfactants on the characteristics of the bubbles produced. Based on the results of this investigation, the following observations can be made:

1. Increases in the injection pressure of air lead to significant increases in the average bubble diameter produced.
2. Increases in the injection pressure of air lead to a wider distribution of bubble sizes produced.
3. At the highest injection pressure (11.0 kPa), the size distribution of bubble diameters increased, with the smallest bubble produced being approximately three times larger than the smallest bubble produced at 8.3 kPa.
4. Bubble coalescence occurs even in very large diameter (27.0 mm) particulate materials.
5. Bubble diameters produced in porous media decrease as the diameter of the particulate material increases.
6. Less bubble coalescence occurred in elliptically shaped particulate materials than in spherically shaped ones.
7. Surfactants in the aqueous systems decrease the average bubble diameter produced and also produce more uniform bubble sizes.
8. Surfactants in aqueous/particulate media systems decrease the average bubble diameter and produce a narrower range of bubble sizes than do surfactant free systems.

ACKNOWLEDGMENTS

Thanks to Carl T. Herakovich for the use of his long-distance microscope and to James E. Danberg for his assistance with the experimental setup. Partial financial support for this research was provided by the University of Virginia. This support is gratefully acknowledged.

APPENDIX. REFERENCES

Baker, R. S., Hayes, M. E., and Frisbie, S. H. (1995). Evidence of preferential vapor flow during in situ air sparging. *In situ aeration: Air sparging, bioventing, and related remediation processes*, Battelle Press, Columbus, Ohio, 63–73.

Bruell, C. J., Marley, M. C., and Hopkins, H. H. (1997). ''American Petroleum Institute in situ air sparging database.'' *J. Soil Contamination*, Vol. 6, No. 2, 169–185.

Burns, S. E., Yiacoumi, S., and Tsouris, C. (1997). ''Microbubble generation for environmental and industrial separations.'' *Separations and Purification Technol.*, Vol. 11, 221–232.

Burns, S. E., Yiacoumi, S., Frost, J. D., and Tsouris C. (1998). ''Application of digital image analysis for size distribution measurements of microbubbles.'' *Proc. Engrg. Found. Conf. on Imaging Technologies: Techniques and Applications in Civ. Engrg.*, Davos, ASCE, Reston, Va., 100–107.

Chen, M.-R., Hinkley, R. E., and Killough, J. E. (1996). ''Computed tomography imaging of air sparging in porous media.'' *Water Resour. Res.*, Vol. 32, No. 10, 3013–3024.

DOCKET ALARM

Explore Litigation Insights

Docket Alarm provides insights to develop a more informed litigation strategy and the peace of mind of knowing you're on top of things.

Real-Time Litigation Alerts

Keep your litigation team up-to-date with **real-time alerts** and advanced team management tools built for the enterprise, all while greatly reducing PACER spend.

Our comprehensive service means we can handle Federal, State, and Administrative courts across the country.

Advanced Docket Research

With over 230 million records, Docket Alarm's cloud-native docket research platform finds what other services can't. Coverage includes Federal, State, plus PTAB, TTAB, ITC and NLRB decisions, all in one place.

Identify arguments that have been successful in the past with full text, pinpoint searching. Link to case law cited within any court document via Fastcase.

Analytics At Your Fingertips

Learn what happened the last time a particular judge, opposing counsel or company faced cases similar to yours.

Advanced out-of-the-box PTAB and TTAB analytics are always at your fingertips.

API

Docket Alarm offers a powerful API (application programming interface) to developers that want to integrate case filings into their apps.

LAW FIRMS
Build custom dashboards for your attorneys and clients with live data direct from the court.

Automate many repetitive legal tasks like conflict checks, document management, and marketing.

FINANCIAL INSTITUTIONS
Litigation and bankruptcy checks for companies and debtors.

E-DISCOVERY AND LEGAL VENDORS
Sync your system to PACER to automate legal marketing.